Author Manuscript

Author Manuscript

Author Manuscript

Author Manuscript

HHS Public Access

Author manuscript

Lab Chip. Author manuscript; available in PMC 2019 December 04.

Published in final edited form as:

Lab Chip. 2018 December 04; 18(24): 3733–3749. doi:10.1039/c8lc00818c.

Functional TCR T cell screening using single-cell droplet microfluidics

Aude I. Segaliny[a,b,c,d,e,f,#], **Guideng Li**[g,h,i,#], **Lingshun Kong**[a,b,c,d,e,f], **Ci Ren**[a,b,c,d,e,f], **Xiaoming Chen**[a,b,c,d,e,f], **Jessica K. Wang**[g], **David Baltimore**[g,#], **Guikai Wu**[j,*], and **Weian Zhao**[a,b,c,d,e,f,*]

[a]Sue and Bill Gross Stem Cell Research Center, University of California, Irvine, Irvine, CA 92697, U.S.A.;

[b]Department of Pharmaceutical Sciences, University of California, Irvine, Irvine, CA 92697, U.S.A.;

[c]Chao Family Comprehensive Cancer Center, University of California, Irvine, Irvine, CA 92697, U.S.A.;

[d]Edwards Life Sciences Center for Advanced Cardiovascular Technology, University of California, Irvine, Irvine, CA 92697, U.S.A.;

[e]Department of Biomedical Engineering, University of California, Irvine, Irvine, CA 92697, U.S.A.;

[f]Department of Biological Chemistry, University of California, Irvine, Irvine, CA 92697, U.S.A.;

[g]Division of Biology and Biological Engineering, California Institute of Technology, Pasadena, CA 91125, U.S.A.;

[h]Center of Systems Medicine, Institute of Basic Medical Sciences, Chinese Academy of Medical Sciences & Peking Union Medical College, Beijing 100005, China;

[i]Suzhou Institute of Systems Medicine, Suzhou 215123, China;

[j]Amberstone Biosciences LLC, Irvine, CA 92617, U.S.A.;

Abstract

Adoptive T cell transfer, in particular TCR T cell therapy, holds great promise for cancer immunotherapy with encouraging clinical results. However, finding the right TCR T cell clone is a tedious, time-consuming, and costly process. Thus, there is a critical need for single cell technologies to conduct fast and multiplexed functional analyses followed by recovery of the clone of interest. Here, we use droplet microfluidics for functional screening and real-time monitoring of single TCR T cell activation upon recognition of target tumor cells. Notably, our platform includes a tracking system for each clone as well as a sorting procedure with 100% specificity validated by

[*]**Corresponding authors**: Dr. Weian Zhao, Sue & Bill Gross Hall CIRM Institute, 845 Health Sciences Road, Suite 3027, Irvine, CA, USA 92697, Office Phone: 949-824-9744, weianz@uci.edu, Or Dr. Guikai Wu, Amberstone Biosciences LLC, 23181 Verdugo, Suite 106, Laguna Hills, CA, USA 92653, george@amberstonebio.com.

Author contributions

Conceptualization, A.I.S., G.L., G.W. and W.Z.; Methodology, A.I.S., G.L., L.K., C.R., X.C. and G.W.; Investigation, A.I.S, G.L., L.K., C.R., and J.K.W.; Analysis, A.I.S.; Writing: Original Draft, A.I.S and W.Z.; Editing, A.I.S., G.L., L.K., X.C., J.K.W., D.B., G.W. and W.Z.; Supervision, A.I.S., D.B., G.W. and W.Z.

[#]Co-first authors

Author Manuscript Author Manuscript Author Manuscript Author Manuscript

downstream single cell reverse-transcription PCR and sequencing of TCR chains. Our TCR screening prototype will facilitate immunotherapeutic screening and development of T cell therapies.

Graphical Abstract

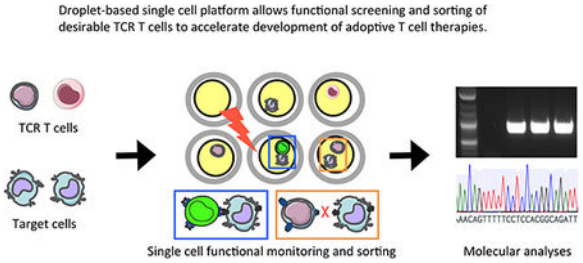

Introduction

There have been an estimated 1,735,350 new cancer cases diagnosed and 609,640 cancer deaths in the United States in 2018, as reported by The American Cancer Society. Most cancers, in particular at advanced stages, remain untreatable. Recent advances in immunotherapy that focus on re-boosting a patient's own immune system brought new hopes for cancer patients, with promising results against leukemia, lymphoma and advanced melanoma[1]. One of the most powerful therapeutic strategies used in cancer immunotherapy is adoptive T cell transfer. There are three types of adoptive T cell therapy: Tumor Infiltrating Lymphocytes (TILs), T cells expressing Chimeric Antigen Receptor (CAR T) and T cells expressing engineered T Cell Receptor (TCR T). These strategies generally involve isolating a patient's own T cells, activating or engineering them to be "armed" against cancer ex vivo, expanding those cells and finally re-injecting them into the patient[2, 3]. TILs require a fresh tumor biopsy to isolate a few reactive T cells leading to an anti-tumor response, whereas CAR T[4] or TCR T[5] cells are engineered from the patient's peripheral blood mononuclear cell. While both CAR T and TCR T cells are compatible with universal cell therapy and able to induce potent anti-tumor response, TCR T cells display several unique properties that make them particularly appealing in treating challenging solid tumors. First, while CAR T cells target surface tumor antigens, TCR T cells can also target the intracellular proteome through human leukocyte antigen (HLA) presentation, meaning TCR T cells can recognize a wide range of tumor antigens that are not restricted to membrane expression, including neo-antigens. In addition, TCR T cells match patient HLA alleles, which avoids rejection following transplantation. TCR used to engineer T cells also have adjustable affinity compared to the native TCR[6], allowing fine-tuning between potency and self-reactivity. Finally, TCR T cells have a better tumor penetrance and distribution within the tumor, whereas CAR T cells tend to stick at the tumor periphery due to the recognition of surface antigens, making TCR T cells more efficient in treating solid tumors[7, 8].

However, the current methods to develop adoptive T cell therapies are inefficient, time-consuming and expensive (resulting in costly T cell products: as an example, one infusion of engineered T cells can cost half a million dollars)[8]. In particular, the highly complex T cell

Author Manuscript Author Manuscript Author Manuscript Author Manuscript

repertoire poses a unique challenge in quickly and reliably identifying the rare T cells of interest that are able to both recognize tumor antigens and display a functional anti-tumor response[9]. There are billions of different TCR clonotypes, but only a few are specific for certain antigens[10, 11]. The conventional bulk and population-based T cell analysis only gives an averaged and overall outcome, which mask molecular details such as variations in T cell activation[12, 13], as well as interesting properties of a single clone, in particular when it is a rare one[14–16]. A major bottleneck of TCR T cell therapy discovery resides in TCR cell cloning, which takes weeks of work and several limited dilutions. As a result, single cell technologies are needed to dissect complex heterogeneity of T cells and to recover the clones or sequences of interest in order to facilitate discovery of adoptive T cell therapies[2, 10, 17, 18]. Unfortunately, conventional single cell analysis methods[19–21] relying on fluorescence-activated cell sorting (FACS) combined with single cell PCR and Sanger sequencing, for example, are typically not comparable with real-time, functional monitoring of single cells (for *e.g.* T cell activation, tumor cell killing, cytokine release), and are associated with a loss of diversity (only a few hundreds of clones identified over a million of potential clones)[19–22].

The rapid expansion of the microfluidics field has provided new tools to study single cell biology in high throughput[23, 24] with features including *in situ* PCR[25–27], sequencing[28–33], secretome analysis[34–37], cell-cell interactions[38–42], multiplexed biological responses[43], screening of displayed libraries[44], protein engineering[45], and therapeutic screening (for drugs[46], antigen specific T cells[14, 47–49], CAR-T cell products[50] and antibodies[51–60]). In particular, droplet microfluidics separates individual cells into oil droplets with tiny volume (picoliter to nanoliter range), thus making a potent platform to precisely dissect complex immune cell response at the single cell level that could not be obtained otherwise from population-based assays[23]. Droplet based-assays possess multiple advantages: they are readily available, easy to use, and amenable for high-throughput cell screening and sorting (thousands of droplets per second) while protecting cells from the shear forces[24]. Since it requires very little cell input and the whole sample is encapsulated with minimal loss, precious and limited samples such as blood or tumor biopsies could be effectively screened. In addition, droplet chemistries are compatible with mammalian cell biology, keeping cells viable in droplets for up to four days[61]. Moreover, the very small volume of the droplet increases the sensitivity thus decreasing the time for analysis (*e.g.* for the detection of secreted proteins), but also improving the signal/noise ratio of various assays. In addition, multi-functional screening can be performed on single cells in droplets, with the measurement of multiple parameters at once, such as cell surface protein expression or secreted molecules. In addition, this type of phenotypic screening can be done in real time with a precise spatio-temporal control over cell partners and other environmental factors. Therefore, droplet microfluidics is a versatile technology that has been applied for immunotherapy discovery. For instance, primary B cells from immunized mice were functionally screened using droplets in real-time, with a fast detection of antibody secretion and high-throughput[59]. This eliminates the need to first go clonal and expand each clone for downstream functional assays that results in the loss of precious clones associated with conventional methods such as hybridoma or yeast display[22, 62]. Moreover, droplets have also helped to gain more insight in the biology of immune cells such as T cells, natural killer

Author Manuscript Author Manuscript Author Manuscript Author Manuscript

cells or antigen presenting cells by multiplexing different parameters that are simultaneously assessed in droplets. For instance, Konry *et al.* adopted droplet systems to characterize a variety of immune cells with respect to their dynamic activation, cytokine production, cell-cell interaction and target cell killing[34, 38–40, 48]. Chokkalingam, *et al.* used droplet technology combined with flow-cytometry to sort single activated T cells secreting IL-2, IFN-γ and TNF-α[37]. McDaniel *et al.* also demonstrated high-throughput sequencing in less than 12 hours on millions of single T cells while keeping the pairing of both TCR chains (α/β or γ/δ)[63], which is usually lost in bulk sequencing where all the chain sequences are obtained individually[10, 11].

In this study, we have adopted and further developed droplet microfluidics for functional screening and real-time monitoring of activation of TCR T cells upon recognition of target tumor cells with the goal of quickly identifying candidate T cell therapeutics for future cancer treatments, and recover their TCR sequence. Notably, our platform includes a tracking system for each individual clone and a sorting procedure to recover the clones of interest for downstream analysis. By co-encapsulating in droplets TCR T cells together with target cells expressing the complex HLA/NY-ESO-1 antigen peptide as a model system[64–66] (Fig.1A, B), we demonstrated that we could 1) visualize the dynamic of TCR T cell interaction with target cells over time, 2) perform real-time analysis of TCR T cell activation kinetics, 3) dissect TCR T cell heterogeneity among the population of interest, 4) sort the TCR T clone of interest using laser-based cavitation, and finally 5) perform downstream molecular analysis using single cell RT-PCR and sequencing TCR sequences to confirm they indeed match with target antigens with a specificity of 100% (absence of false positives).

Experimental

Reagents

Fetal bovine serum (FBS) was purchased from Atlanta Biologicals. 7.5% sterile bovine serum albumin solution (BSA), 4-(2-Hydroxyethyl) piperazine-1-ethanesulfonic acid (HEPES), 1H,1H,2H,2H-perfluoro-1-octanol, OPTIPREP and β-mercaptoethanol were purchased from Sigma-aldrich. RPMI 1640, IMDM (GlutaMAX Supplement), MEM Non-Essential Amino Acids (NEAA), sodium pyruvate, 200g/L glucose solution, Penicillin Streptomycin solution and cell tracking fluorescent dyes were purchased from Fisher Scientific. Assorted Food Color (red, green and blue) was obtained from McCormick. L-glutamine was purchased from Genesse. RNAsin Plus RNase Inhibitor was obtained from Promega.

Cell lines

Jurkat E6.1 and K562 cells were purchased from the American Type Culture Collection, and were respectively cultured in RPMI 1640 medium supplemented with 10% (v/v) FBS, 10mM HEPES, 50μM β-mercaptoethanol, 1X NEAA and 1mM sodium pyruvate, and IMDM medium supplemented with 10% (v/v) FBS. All cells were cultured at 37°C with 5% atmospheric CO_2. MART-1 and NY-ESO-1 TCR T reporter cells were generated by transducing Jurkat E6.1 T cells with a retroviral vector encoding the MART-1 (F5)- or NY-ESO-1 (1G4)- TCR gene and a lentiviral vector encoding NFAT-GFP reporter gene. NY-

Author Manuscript Author Manuscript Author Manuscript Author Manuscript

ESO-1$^+$ target cells were generated by transducing K562 cells with a lentiviral vector encoding the relevant single-chain trimer, composed of a single polypeptide chain with a linear composition of antigenic peptide (NY-ESO-$1_{157–165(C165V)}$), β2-microglobulin, and HLA-A2 domains via flexible GS linkers. Cells expressing the transgenes were selected using puromycin and sorted by flow-cytometry.

Flow-cytometry

50,000 TCR T cells were plated with varying ratios of target cells (5:1, 1:1 and 1:5 TCR T cell:Target cell), and cells were collected at different time-points to analyze the percent of activated TCR T cells (eGFP$^+$) using flow-cytometry. Following collection, cells were washed and read in PBS on an Accuri C6 flow cytometer (BD Biosciences, San Jose, CA, USA). The percent of eGFP$^+$ cells was gated in the FL-1 channel after gating for single cells (FSC-A/FSC-H) within the cell population (FSC-A/SSC-A), and gating out the target cells to quantify the percent of TCR T cells that get activated. 20,000 events were collected from the single cell gate for analysis.

Fluorescence plate reader assay

50,000 TCR T cells were plated with varying ratios of target cells (5:1, 1:1 and 1:5 TCR T cell:Target cell). The fluorescence signal emitted from the eGFP was collected from a plate reader (Synergy HT, Biotek, Winooski, VT, USA) using a gain of 50, a reading from the top and 485 ±20nm excitation and 528 ±20nm emission filters. The plate reader was set at 37°C, and one reading was done every 2 hours over a total of 12 hours.

Microscope imaging

Imaging was performed using an Eclipse Ti epifluorescent microscope with a 10X objective (Nikon, JPN). Nikon DS-Ri2 color camera (13W) and Lumencor Spectra X light engine with an Andor Zyla 5.5 sCMOS camera (60W) were used for brightfield imaging and fluorescent imaging, respectively. Filters were set as the following: DAPI (excitation 358nm/emission 461nm), FITC (excitation 490nm/emission 525nm) and Cy5 (excitation 649nm/emission 665nm) were used. The exposure time and % of intensity for LED sources were set as the following: DAPI (10ms/5%), FITC (150ms/10%) and CY5 (50ms/5%). The exposure time for brightfield imaging was 100 ms, and the voltage was set at 5V.

Microfluidic chip design and fabrication

Microfluidic chips were made from polydimethylsiloxane (PDMS) polymer (Sylgard 184 elastomer kit; Dow Corning Corp) using the standard soft lithography technique[67]. The fabrication process included three steps: (1) A mask design was made using AutoCAD and printed out from CAD/Art Services, Inc. (CA, USA); (2) A master mold was fabricated on a 4” silicon wafer (IDB Technologies, Wiltshire, UK); All the master molds were fabricated in UC Irvine clean room. The master mold fabrication process can be found here[68]. PDMS with base/curing agent ratio 10:1 was poured onto the master for making microfluidic chips. In details, after fully mixing of the base and curing agent, PDMS was put into a vacuum chamber for degassing. Then, the degassed PDMS was poured onto the silicon wafer in an aluminum foil pan followed by degassing again. After that, the aluminum pan was put in an

Author Manuscript Author Manuscript Author Manuscript Author Manuscript

oven to bake for at least 2 hours at 95°C. Once the PDMS mold was cured, it was peeled off and cut into the desired shape. Reservoirs were punched into the PDMS by a 1.5mm sized biopsy punch (Kay Industries Co., Tokyo, Japan). Tape was used to remove any dust and particles on the PDMS mold. Then, the PDMS mold was bonded to a glass slide after air plasma treatment in a plasma cleaner (Harrick Plasma, USA). The PDMS channel becomes hydrophilic after plasma treatment. In order to make it hydrophobic for generating aqueous droplets, the PDMS microfluidic chip was put into a 95°C oven for at least 24 hours to bake before use.

Droplet generation

TCR T cells and target cells were resuspended in RPMI 1640 medium supplemented with 20% (v/v) FBS, 1% P/S, 10% OPTIPREP and additional glucose and amino acids. A flow-focusing generator (width=65μm, height=100μm and orifice width=45μm) was used to encapsulate individual TCR T cells and target cancer cells into single droplet. HFE7500 fluorocarbon oil (Novec™, 3M, USA) containing 2.2% by weight fluoro-surfactant (PFPE 5000-PEG900, Creative PEGWorks, USA) was used as the continuous phase. The two cell suspensions (TCR T cells and target cells) co-flowing into the microchannel from two separate reservoirs were used as the disperse phase. The flow rates of TCR T cell suspension, target cell suspension, and oil were set as 10μL/min, 10μL/min, 40μL/min respectively to generate D=120μm sized droplets. The flow ratio between the dispersed phase and the continuous phase was slightly adjusted to obtain the desired droplet size.

Cell labeling and distribution in droplets

Cell distribution in droplet and co-encapsulation efficiency were evaluated by fluorescent imaging after labeling NY-ESO-1 TCR T cells, MART-1 TCR T cells and NY-ESO-1^+ target cells using spectrally distinct cell tracking dyes with the following excitation/emission peak values: 405/450nm, 495/515nm and 630/661nm.

Droplet trapping, incubation and imaging

Generated droplets were directed into an improved version of our inverted floating droplet array (iFDA)[68] through a micro-tubing (Inner Diameter ID = 0.5mm, Outer Diameter OD = 1.5mm, Tygon® Microbore Tubing, USA). The iFDA chip contains 10,368 trapping wells, and each trapping well has a diameter of D_{well}=140μm and a height of H_{well}=130μm to ensure that only one droplet is trapped in each well. The gap length between two adjacent trapping wells is L_{gap}=100μm to maximize the number of wells. The channel height (first layer) $H_{channel}$=150μm is set slightly larger than the droplet diameter to allow single layer of droplets to pass through the chamber. The iFDA chip is a two layers fabrication; the entire chip is divided into 8 sections to reduce the dead zone, with each section contains 162 by 8 wells (1,296 wells). Once all of the trapping wells were filled with droplets, the iFDA chip was disconnected from the droplet generator, and extra droplets inside the iFDA chamber were removed by injecting fluorinated oil (HFE7500) with a flow rate of 200μL/min. Theoretically, the majority of droplets (>90%) injected into the iFDA chip can be trapped by tilting the chip back and forth. Next, the iFDA chip was placed inside a live cell chamber (H301-NIKON-TI-S-ER, OKO-LAB, Italy) set with 95% humidity, 5% CO2 and 37.5°C. The iFDA chip was held using a single slide 1”x3” chamber slide, 1xGS-M (OKO-LAB,

Author Manuscript Author Manuscript Author Manuscript Author Manuscript

Italy) on the Nikon microscope stage for incubation over 9 hours. Imaging was automatically performed every 3 hours on 20 fields of view each containing 30 droplets, randomly selected and evenly distributed across the iFDA chip to limit photobleaching in the selected areas. In addition, although most cells sunk to the bottom of the droplets, images were captured using 5 z-stacks (from −10μm to +10μm with 5μm for each step) to make sure cells were captured in the best focal plane with the maximum intensity.

Cell viability in droplets

To test cell viability in droplets at the different time-points, droplets were merged and broken using 1H,1H,2H,2H–perfluoro-1-octanol (PFO; Sigma-Aldrich,USA) in order to recover the cells trapped inside droplets. Briefly, 5μL of PFO was added to 10μL of droplets as a demulsifier for 5minutes, then 50μL of cell culture media (RPMI 1640). Once most droplets were merged with culture media and the cell suspension separated from the oil phase, 10μL of Trypan Blue (Corning, USA) was added to 10μL of cell suspension to count the number of viable cells.

Droplet sorting

A UV-laser microdissection microscope (Zeiss PALM MicroBeam, Germany) was used for sorting out droplets from iFDA chip under brightfield (5X magnification) through heat-induced cavitation. The microscope was kept at 27°C while a heating lamp (43W, Halogen lamp, Sylvania) was added above the iFDA chip to heat the oil for bubble generation. The 355nm UV-laser was focused on the edge of the target trapping well to heat up the carrier oil while avoiding damage to the cells inside the droplet, and was set at the following parameters: focused beam diameter ~0.6μm, pulse energy above 90 μJ and pulse duration below 2 nanoseconds after passing the objective. A bubble was then created inside the trapping well due to heat-induced cavitation, expelling the droplet out of the trapping well. After that step, additional carrier oil was injected inside the iFDA chip with a flow rate of 400 μL/min to flush the droplet into a recovery chamber. Meanwhile, the created bubble vanished due to the refreshment of cooling carrier oil, thus allowing another droplet to be sorted.

Droplet dispensing

The recovery chamber dimensions (40 mm × 15 mm, length × width) made it possible to slow down the speed of the flowing droplet and trap it. The droplet inside the chamber was visualized under a large field of view (12.9mm × 17.1mm) microscope (Industrial Inspection Zoom Monocular Microscope, Amscope), and then slowly pushed into the outlet of the recovery chamber to be pipetted out. After double-checking that the single cell was sucked into the pipette under the large field of view microscope, the single cell was transferred into a PCR tube.

Droplet lysis and RNA extraction.

After droplets were dispensed into PCR tube containing 5 μL of ice-cold lysis buffer (PBS containing 2% BSA and 200U RNAsin/mL), the PCR tube was centrifuged 20 seconds in

Author Manuscript Author Manuscript Author Manuscript Author Manuscript

order to merge the droplet with lysis buffer. After centrifugation, the PCR tube was double checked under the microscope to ensure that the cell was released from the droplet.

Single cell RT-PCR of TCR

Single cells were lysed by freeze-thaw in the presence of RNase inhibitor, and were then immediately flash frozen and stored at−80 °C until use. Upon thawing, the cell lysate from each cell was processed directly into PCR for both α and β chain genes using a OneStep RT-PCR kit (QIAGEN), following the manufacturer's instructions and using the TCR gene-specific primers: 5'-atggcgacgggttcaagaacttc-3'(FW primer targeting TCR leading sequence) and 5'-agattaaacccggccactttcagg-3'(BW primer targeting TCR constant regions). The PCR product was amplified for two additional rounds using the same TCR gene-specific primers. The PCR reactions were purified using the DNA Clean& Concentrator-5 Kit (Zymo Research, Irvine, California), following the manufacturer's protocol.

Sequencing analysis

To verify amplified TCR sequences, sequencing was performed by Retrogen (La Jolla, CA) using the following primers: 5'-attgggtttcacagataactccgttcc-3'(targeting MART-1 TCR) and 5'-atacggatgaacaataaggctggttcc-3'(targeting NY-ESO-1 TCR).

Software, image processing and statistical analysis

The AutoCad (AutoDesk, USA) software was used to design the mask for lithography. Image processing and analysis were done using the NIS Elements Advanced Research package (Nikon, JPN). Fold-changes in eGFP signal were measured for each TCR T cell by normalizing the maximum intensity signal in FITC channel at each time point to the maximum intensity signal at t=0 hour. R (programming language, R Core Team, USA) was used to generate the T cell activation heatmap. GraphPad Prism (GraphPad Software, Inc, USA) was used for plotting graphs and for statistical analysis. Each experiment was performed independently at least in duplicate, with replicates for each condition.

Results & Discussion

Models of TCR T cells and target cells expressing cognate antigens.

As a model in our proof of concept for screening specific TCR T cells that recognize tumor antigens, we used NFAT-eGFP reporter Jurkat cells[69] that expressed either MART-1 or NY-ESO-1 specific TCR (F5-TCR and 1G4-TCR, further designated as "MART-1 TCR T cells" and "NY-ESO-1 TCR T cells" in the study), as well as K562 cells that expressed peptides from the NY-ESO-1 antigen with MHCI complex (designated here as "target cells"). We first generated Jurkat T cells containing an eGFP gene expressed under the control of the NFAT/AP-1 response elements, which plays a major role in TCR signaling[13, 69]. These T cells were then transduced either with a retroviral vector that delivered the HLA-A2/MART-$1_{26–35}$-specific TCR[5, 70] or with a HLA-A2/NYESO$1_{157–165}$-specific TCR[6]. In parallel, K562 cells were transduced with a lentiviral vector that delivered a single-chain trimer of HLA-A2/NYESO-$1_{157–165(C165V)}$[6]. When NY-ESO-1 TCR T cells come in contact

Author Manuscript Author Manuscript Author Manuscript Author Manuscript

with target cells and recognize their cognate antigen, the TCR signaling pathway become activated thus inducing eGFP expression inside the cells, both in the nucleus and cytoplasm (as conceptually illustrated in Fig.1A). In contrast, MART-1 TCR T cells do not get activated upon contact with NY-ESO-1$^+$ target cells.

Specific activation of NY-ESO-1 TCR T cells in the presence of NY-ESO-1$^+$ target cells in a time and target cell concentration dependent fashion in bulk.

We first plated MART-1 TCR or NY-ESO-1 T cells at different ratios together with the target cells (5:1, 1:1, or 1:5 TCR T cells for target cells) and measured eGFP$^+$ cells using flow-cytometry to determine the percent of cells that got activated. When co-cultured with target cells expressing the NY-ESO-1 antigen, negative control MART-1 TCR cells did not get activated, even when plated with 5 times more target cells than TCR T cells (Fig.2A). By contrast, NY-ESO-1 TCR cells got activated in a time and target cell concentration dependent fashion. More than 80% of the NY-ESO-1 TCR cell population got activated after 24 hours in all tested cell ratios between TCR T cells and target cells, and when NY-ESO-1 TCR T cells were plated at a ratio 1:1 to 1:5 with NY-ESO-1$^+$ target cells, almost 80% of the cells got activated after 6 hours (Fig.2B). This time-dependent T cell activation is most evident at TCR T cell:Target cell ratio of 5:1 where target tumor cell is scarce and T cells take time to move around to encounter a tumor cell to be activated. Indeed, at TCR T cell:Target cell ratios of 1:1 and 1:5 where tumors cells are in excess, the percentage of T cells got activated are less dependent on cell ratios, especially at 6 hour incubation time or longer. Then, using the same plating ratio, we measured the fluorescence intensity of the eGFP over time using a plate reader (485±20nm excitation and 528±20nm emission filters) to evaluate the activation kinetics of the bulk population. As expected, we did not detect any eGFP expression using MART-1 TCR T cells, as they do not recognize the target cells (Fig. 2C). We even observed a small decrease of the overall level of background fluorescence, which is likely due to the photobleaching of the residual eGFP, due to promoter leakiness. Despite this photobleaching effect, we observed an increase of the eGFP expression over time using the NY-ESO-1 TCR T cells which started plateauing at 12 hours (Fig.2D), consistent with similar Jurkat reporter lines[69]. The more NY-ESO-1$^+$ target cells plated with NY-ESO-1 TCR T cells, the stronger the total observed fluorescence was, likely due to that more target cells lead to both increased number of activated NY-ESO-1 TCR T cells and stronger, more sustained activation of intracellular signaling for a particular TCR T cell (Fig. 1A). While this bulk assay functionally validated our cell line pairs, important information regarding cell heterogeneity and TCR activation at the single cell level cannot be revealed.

Co-encapsulation of TCR T cells and target cells using droplet microfluidics.

To study TCR activation upon antigen recognition at the single cell level, we compartmented one TCR T cell together with target cell(s) using droplet microfluidics. A flow-focusing droplet generator was used to encapsulate individual TCR T cells and target cells into single droplets (Fig.3A–B). HFE7500 fluorocarbon oil containing 2.2% by weight fluoro-surfactant (PFPE 5000-PEG900), which helps mammalian cells remain healthy[61], was used as the continuous phase, which is designated as “oil” hereafter for simplicity. Two cell suspensions co-flowing into the microchannel from two separate reservoirs were used as the disperse phase, with one containing NY-ESO-1 TCR T cell (cells of interest) spiked with

Author Manuscript Author Manuscript Author Manuscript Author Manuscript

another type of TCR T cells against MART-1 antigen (unwanted cells) at a 1:1 ratio, and the other containing NY-ESO-1^+ target cancer cells (Fig.3A). The two cell suspensions were separated before being injected into the flow-focusing device in order to prevent cell-cell interaction (cell activation) prior to droplet generation. To better visualize the two cell suspensions and confirm the 1:1 distribution within the channel when mixing at the T-junction, TCR T cells suspension was dyed in blue and target cells in red for the initial set of experiments. The channel dimensions of the flow focusing geometry were designed with width=65μm, height=100μm, and orifice width=45μm for generating droplets with diameter of D=120μm, which corresponds to about 1nL volume (904.8pL). Droplet diameter was very consistent over 48 droplets randomly measured, with a mean of 119.42±1.67μm (see Fig.4C, below, for a representative image). This droplet size was chosen since it contained sufficient nutrients to maintain good cell viability over an incubation of 9 hours (Suppl. Fig.1). Specifically, we separately encapsulated each cell type in droplet (MART-1 TCR T cells, NY-ESO-1 TCR T cells, NY-ESO-1^+ target cells), and we also encapsulated the NY-ESO-1 TCR T cell/NY-ESO-1^+ target cell pairs to measure cell viability over time. After 3, 6 and 9 hours, the cells were recovered by breaking the droplets using 1H,1H,2H,2H-perfluoro-1-octanol, and the percent of viable cells was counted. In each condition, the cell viability remained above 90% over 9 hours (Suppl. Fig.1).

Single cell (co)encapsulation efficiency

To screen for single TCR T cells, we had to minimize the number of droplets containing more than one TCR T cell. In randomly dispersed aqueous cell suspensions, the probability that a droplet contains k cells follows Poisson statistics, *i.e.*, $P_{k,\lambda} = \frac{\lambda^k e^{-\lambda}}{k!}$, where λ is the average number of cells per droplet. The average number of TCR T cells per droplet is $\lambda_1=1$ (cell concentration 1.1×10^6 cells/mL) in order to maximize the single cell encapsulation rate, while the average number of target cells per droplet is $\lambda_2=1.5$ (cell concentration 1.66×10^6 cells/mL) to ensure that most of the droplets contain one or multiple target cells, because a single droplet containing one NY-ESO-1 (or MART-1 TCR T cell) and multiple target cancer cells is acceptable for T-cell activation. Indeed, bulk data confirmed that having more than one target cell for one TCR T cell led to a better activation compared to a 1:1 ratio (Fig. 2). We thus decided to maximize droplets containing 1:1 pairs and to include droplets up to three target cells but minimize cases where too many cells are encapsulated in one droplet, as it would limit the amount of nutrients accessible to each cell and thus decrease the overall cell viability. Prior to encapsulation, cells were labeled with distinct cell tracking fluorescent dyes. We then encapsulated either one TCR T cell type (NY-ESO-1 TCR) with target cells, or a cell mixture of both TCR at a 1:1 ratio with target cells. To ensure that the cell distribution was following Poisson statistics, we loaded the generated droplet on the chip containing the trapping wells, and imaged the chip. In a field of view containing 128 droplets, we can see several droplets containing both one NY-ESO-1 TCR cell (green) and one or more target cells NY-ESO-1^+ (orange) (Suppl. Fig.2A). We then quantified the different categories of droplets containing 1:1 NY-ESO-1 TCR cell: target cell, 1 NY-ESO-1 TCR cell and more than 1 one target cell (1:>1), or the ones not matching those criteria (other category: empty droplets, containing NY-ESO-1 TCR cells alone, target cells alone, or more than one NY-ESO-1 TCR cell with target cells). Those quantifications were done on

Author Manuscript Author Manuscript Author Manuscript Author Manuscript

three independent experiments, with ~700 droplets analyzed for each of them. The distribution was close to the Poisson distribution, although for the % of droplets containing one NY-ESO-1 TCR cell and more than one target cell, the experimental data (7%) appeared slightly lower than the theoretical one (16.2%) (Suppl. Fig.2B). After on chip mixing of NY-ESO-1 TCR cells and MART-1 TCR cell at a 1:1 ratio and following encapsulation with target cells, we observed on chip the presence of both pairs of interest: the negative ones (one MART-1 TCR cell with one or more target cells) and the positive ones (one NY-ESO-1 TCR cell with one or more target cells) (Suppl. Fig.1C). Despite an acceptable distribution, the number of pairs of interest was lower than what was expected according to the Poisson statistics (Suppl. Fig.1D). This could be attributed to cell aggregation during droplet generation although we used a density medium in the encapsulation medium to match cell density and avoid sedimentation.

The inverted floating droplet array (iFDA) allows monitoring of individual droplet and single TCR T cells.

To monitor each individual TCR T cell in a droplet over time, we used an inverted floating array (iFDA) containing tens of thousands of trapping wells, which was adapted from our previous work[68] (Fig.4). Despite its limited throughput, this device gave us the unique advantage of being able to monitor TCR T cell interaction with target cells at the single cell level. Not only did the iFDA allow us to observe T cell activation kinetics of each TCR T cell paired with target cells through eGFP expression, but it also allowed us to recover the droplet of interest for further downstream analysis. Once confirmed under the microscope that droplet size was correct and uniform, droplets were directed from the flow-focusing device into the iFDA through a micro-tubing, where they got trapped into microwells due to buoyancy (Suppl. Video 1). Compared to our previously published design[68], the new chip used in this paper was divided into 8 sections to reduce the dead zone so that droplets could flow into every trapping well. Each section contained 162×8=10,368 wells. Each trapping well of the chip had a diameter of D_{well} =140μm, and height of H_{well} =130μm to ensure only one droplet could be trapped in each well without being flushed out by the carrier oil (Fig. 4A). The gap length between two adjacent trapping wells was L_{gap}=100μm to maximize the number of wells, while considering technical limitation of the fabrication process. The channel height (First layer, Fig.4B) was set slightly larger than the droplet diameter $H_{channel}$=150μm to allow the single layer of droplets to pass through the chamber. In order to track the activated TCR T cells and further sort the droplet of interest out, we labeled the trapping wells with specific numbers (for *e.g.* row E column 24, Fig.4C). As illustrated in Fig.4C, droplets of homogenous size occupied all the iFDA wells. Theoretically, tilting the chip back and forth could trap more than 90% of droplets injected into the iFDA chip. However, since sample loss was not critical for this specific project (unlimited samples and larger number of droplets than well number: 300,000 *v.s.* 10,000), droplets were loaded in excess to save time: indeed, it only took about 1 minute to fully load the iFDA. Once all of the trapping wells were filled with droplets, the iFDA chip was disconnected from the droplet generator, and extra droplets inside the iFDA were removed by injecting oil with a flow rate of 200μL/min without disturbing the trapped droplets, which took about 10 seconds (Suppl. Video 1). As droplets were found to evaporate over time during incubation, especially for those trapped in the microwells close to the inlet and outlet, we set the inlet

Author Manuscript Author Manuscript Author Manuscript Author Manuscript

and outlet 5mm away from the microwell array. In addition, the PDMS chip was made with a thickness of at least 8mm to reduce droplet evaporation. The diameter of droplets reduced from 120μm at the beginning of incubation to around 100μm for most of the droplets, and to around 70μm diameter for droplets close to the inlet/outlet and the edge of the iFDA after 9 hours incubation (**data not shown**). In addition, since both the inlet and the outlet were blocked during incubation, droplet evaporation created some vacuum inside the iFDA, leading to air coming into the chamber, which repelled droplets from the microwells. To compensate the loss of pressure inside the chamber, a pressure pump was connected to the inlet with a pressure of 80 mbar and the tubing filled with carrier oil.

NY-ESO-1 TCR T cells are specifically activated, though to a different extent, in the presence of NY-ESO-1$^+$ target cells

To characterize the T cell activation in a droplet, we performed experiments where we encapsulated matching NY-ESO-1 TCR cells with NY-ESO-1$^+$ target cells (positive pairs, further designated as “positives”), or MART-1 TCR cells with the target cells (negative pairs, further designated as “negatives”). Once droplets were loaded in the trapping wells and additional droplets were flushed out, the iFDA was incubated over 9 hours in a live cell chamber with 95% humidity, 5% CO_2 at 37.5°C, and imaged for both bright field and fluorescence every three hours. 20 fields of view covering the entire chip were taken at 10X magnification with 5 z-stacks of 5μm set around the focal plane at T0 in order to capture all cells in droplets at their best focus. Each field of view contained 30 droplets, and was randomly selected apart from the other ones to limit photobleaching in the selected areas. We noticed that quickly after encapsulation and droplet loading, TCR T cells and target cells started interacting, and usually remained in contact during the whole experiment despite the stage movement (Suppl. Video 2). In addition, because the density of the encapsulation medium was still slightly lower than the cell density, the TCR cell and the target cell sank to the bottom of the droplet, facilitating cell-cell interaction (Fig.4C, image on the right for example), which is necessary in order to trigger TCR signaling. We confirmed the absence of T cell activation for TCR T cells encapsulated alone, and for MART-1 TCR cells encapsulated with target cells (Fig.5A, B, C). Furthermore, NY-ESO-1 TCR T cells started expressing eGFP 3 hours after being in contact with target cells, thus confirming the TCR T cell ability to get activated by matching tumor antigen presented by target cells (Fig.5D). Similar to the bulk data (Fig.2), the activation significantly increased after 6 hours. For each of the 4 independent experiments, droplets of interest were randomly picked on the criteria of containing one TCR cell and one to three target cells; 90 droplets were analyzed in total for both negative and positive pairs. To visualize the activation of TCR T cells in each analyzed droplet, we plotted the results into a heat map where each row showed one single droplet, and the activation level was represented with a green gradient (activation fold change compared to t=0 hours ranging from 0.72 to 69.4; pale yellow=lowest activation, dark green=strongest activation, Fig.5E). For the majority of activated NY-ESO-1 TCR T cells, the activation was generally stronger after 9 hours than that after 3 and 6 hours. Interestingly, approximately 30% of the cells did not get activated as shown by the rows on the heat map that remain pale yellow or light green after 6 and 9 hours (Fig.5E), which was more than that in bulk (>80% activated TCR T cells after 9 hours, Fig.2A). Indeed, within a same area where TCR T cells interacted with target cells in droplets containing positive

Author Manuscript Author Manuscript Author Manuscript Author Manuscript

pairs, we could observe both cases of strong T cell activation or no activation (Suppl. Video 2). In addition, some cells got strongly activated after 6 hours but the eGFP signal decreased at 9 hours, as indicated on the heat map by the red arrow (Fig.5E), which was usually associated with a loss of cell viability. The heat map has the advantage of showing the heterogeneity at the single cell level. As T cell activation was generally stronger after 9 hours, we focused on that time-point to analyze the different populations: negatives (TCR cells alone or MART-1 TCR T cells + target cells) and positives (NY-ESO-1 TCR T cells + target cells). The plotted eGFP fold-change showed a broad variation in T cell activation from one TCR T cell to another, ranging from a 2-fold change in eGFP signal up to a 70-fold change at the end-point for the positive pairs that clearly separated from the negatives (Fig.5F). 50% of the TCR T cells from positive pairs showed a fold increase of >5 at 9 hours. Using the mean eGFP signal of all the negatives, we attempted to determine thresholds at 9 hours for sorting the droplet of interest that contain T cells activated by the target cells. For clarity, we generated a second plot showing eGFP fold-change at 9 hours for negatives and positives including thresholds, with a scale limited to 10 fold-increase instead of 80 (Fig.5G, zoom in of Fig.5F). We set up two thresholds, a lower one ($Mean_{negative\ signal}$ + 2 standard deviations=1.68) and a more stringent one ($Mean_{negative\ signal}$ + 4 standard deviations=2.12) (Fig.5G). The second threshold excluded almost all the negatives, but also limited the number of positives to be included for sorting. From the current data, the lower threshold gave a false positive rate of 4.2% while the stringent one gave 0.6%, but we also missed 1.8% of true positives using that stringent threshold. However, performing kinetics analysis rather than only end-point analysis helped avoid the selection of false positives (*i.e.* better specificity) or the exclusion of true positives (*i.e.* better sensitivity). Indeed, unpaired TCR T cells could have an eGFP fold-increase above 1.68 (less stringent threshold) but not showing good activation kinetics profile. Similarly, positive samples could have a similar level of eGFP expression at the end-point close to the threshold, but actually showed a fairly different activation kinetics profile. As an example, we plotted the activation kinetics of two NY-ESO-1 TCR and MART-1 TCR T cells from negative and positive groups that exhibited similar eGFP level at the 9 hour end-point, but a very strong increase at 6 hours for the TCR T cells from the positive pair prior to losing its signal probably due to loss of viability (Fig. 5H). Overall, those data showed TCR T cell activation generally followed the same kinetics in bulk and in droplets. However, compartmenting TCR T cells in single droplet revealed some key information that are lost in bulk, including variability and heterogeneity in activation with respect to activation strength and kinetic, which allowed us to readily discriminate high and low activators as well as non-activated cells among the positive pairs. Moreover, we demonstrated that using a combination of a less stringent threshold at the end-point and the activation kinetics profile for cells exhibiting low eGFP signals maximized the number of positive droplets to be sorted while avoiding selection of false positives, which are all critical parameters for effectively screening for rare, specific and functional TCR T cells.

TCR T cell sorting and recovery for downstream molecular analysis.

To sort the droplets containing the TCR T cells of interest, we used a UV laser (wavelength 355nm) to generate cavitation in the target wells[71]. The laser beam was focused on the edge of the target trapping well to heat up the carrier oil while avoiding damaging the cells inside

Author Manuscript Author Manuscript Author Manuscript Author Manuscript

the droplet. A bubble was created inside the trapping well due to cavitation and expelled the droplet out of the well. Then, additional carrier oil was injected into the iFDA chip at a flow rate of 400μL/min to flush the droplet of interest into a recovery chamber (Fig.6A, Suppl. Video 3). Meanwhile, the created bubble vanished due to the refreshment of cooling carrier oil, which allowed robust sorting of another target droplet (Suppl. Video 4). The success rate of kicking out target droplets was dependent on the bubble size, which was determined by local temperature. Therefore, the laser power and focal plane had to be thoroughly calibrated. In our experiments, we got a success rate of >90% by using the lowest possible focused beam diameter (~0.6μm), a pulse energy above 90μJ, and a pulse duration below 2 nanoseconds. The recovery chamber was designed with the following length × width dimensions: 40mm × 15mm (Fig.6A), which was able to slow down the moving droplet's speed and trap it. The recovered droplet inside the chamber was tracked under a large field of view (12.9mm × 17.1mm) microscope, and then was slowly pushed into the outlet of the recovery chamber to be pipetted out. After double-checking that single cells were collected into the pipette tip under the microscope, they were dispensed individually into PCR tubes for downstream RT-PCR. The whole process of sorting one droplet took about 15 minutes, the longest step being the generation of the bubble (almost 10 minutes). To demonstrate that we could keep track of the selected droplet along the entire process and that the collected droplet was indeed the one selected for sorting, we dyed droplets with different colors using food dyes, and then loaded a mix of droplets (empty droplets or droplets containing red, blue or green dyes) on the iFDA (Fig.6B). We then sequentially sorted droplets with different colors. As shown in Fig.6C and Suppl.Video 3, we could visualize the colored droplet at different steps of the sorting process, thus confirming we could sort the desired droplets with great confidence.

Determination and confirmation of TCR sequence of target TCR T cells using single cell sequencing.

To demonstrate that we can identify a target TCR T cell from a mixture of cells and then determine their genetic profiles via downstream molecular analyses, MART-1 and NY-ESO-1 TCR T cells were mixed at a 1:1 ratio and co-encapsulated with target cells. The activation kinetics was analyzed over time, and, as previously described, droplets of interest were selected among randomly selected droplets containing 1 TCR T cells and 1–3 target cells (good activation kinetics and eGFP fold-increase above the following threshold after 9 hours: $\text{Mean}_{\text{negative signal}}$ + 2 standard deviations=1.68). We recorded the positions of the droplets of interest then moved the iFDA under the laser-equipped microscope to perform the sorting. Droplets were dispensed in pre-filled PCR tubes with 5μL lysis buffer for RNA extraction containing RNAse inhibitors, and were kept at 4°C the whole time. The entire sorting process was performed in a clean, RNAse free environment. In addition, once a droplet was collected in a PCR tube, we made sure the droplet was fully merging with lysis buffer before flash-freezing the tube, which was kept at −80°C until next step to avoid RNA degradation. We next performed single cell reverse-transcription (RT) and PCR followed by Sanger sequencing to validate that the sorted droplet only contained the cognate NY-ESO-1 TCR T cells (Fig.7A). We performed RT-PCR using universal TCR primers that amplify any TCR sequence present (endogenous TCR, NY-ESO-1 TCR and MART-1 TCR). The success of the RT-PCR reaction from droplets and the specificity of the primers were verified by

Author Manuscript Author Manuscript Author Manuscript Author Manuscript

testing for the positive controls (droplets containing each TCR cell alone or mixed together) and also for the negative controls (empty droplets or droplets containing NY-ESO-1$^+$ target cells alone) (Fig.7B). We did not see any amplification from the empty droplets (lane 1) or the ones containing the target cell alone (lane 2). By contrast, specific amplification was obtained from all droplets containing TCR T cells including MART-1 TCR T cells (lane 3), NY-ESO-1 TCR T cells (lane 4) and both NY-ESO-1 and MART-1 TCR T cells (lane 5). Next, we purified the DNA from the PCR products in the gel, and confirmed the cell content of each droplet through sequencing with primers specific for NY-ESO-1 TCR or for MART-1 TCR, respectively (Fig.7C). Our data validated that our RT-PCR and subsequent primer-specific sequencing protocols can robustly identify specific TCRs (*e.g.*, discriminating between MART-1 and NY-ESO-1 TCRs) on T cells isolated from droplets without the need for further purification and separation from target tumor cells. Next, we ran the same downstream molecular analysis on laser-sorted, positive droplets that are supposed to contain both one NY-ESO-1 TCR T cell and one or more NY-ESO-1$^+$ target cell based on T cell activation kinetics. Among five collected droplets in this feasibility demonstration, the RT-PCR reaction worked for four droplets (80%) (Fig.7D), which was consistent with the typical success rate of single cell PCR[72]. Single cell RT-PCR failure could be due to unsuccessful merging of droplets with the lysis buffer following recovery, or RNA degradation because of laser-heat induced damages. The DNA was then purified from the gel and sequenced using the specific TCR primers previously described. NY-ESO-1 and MART-1 TCRs were confirmed to be positive and negative, respectively, in all four samples (Fig.7E). Thus, we confirmed that 1) we were able to successfully run single cell RT-PCR and sequencing on a single laser-sorted droplet, and 2) all sorted “positive” droplets as determined from the activation kinetics profile contained NY-ESO-1 TCR but not MART-1 TCR with a 100% specificity, thus confirming correct matching between cognate NY-ESO-1 TCR T cells/NY-ESO-1$^+$ target cells.

Discussion

In this paper, we devised a droplet-based platform for performing functional screening of T cells based on real-time monitoring of cell-cell interactions at a single cell level and for downstream identification of their TCR sequences. Microfluidic-based single cell systems represent powerful new tools to study immune cell diversity and quickly identify clones of interest. Compared to other microfluidic systems including a cell pairing device that shows lymphocyte activation at the single cell level with similar throughput (10,000 cells analyzed) but higher cell/antigen pairing efficiency (67%)[73], droplets offer several advantages: 1) cells are protected in droplets from shear stress and laser-induced cavitation[44, 71], and remain viable for up to several days[61], 2) the immune cell secretome (secretion of interferon-γ, granzyme B, *etc.*)[34–37] as well as the transcriptome[25–33] can be analyzed for the same cells, 3) the TCR chain pairing is not lost[20, 31, 63] and 4) droplets with cells of interest can be easily recovered for further molecular analyses and culture expansion and manipulation.

We were able to specifically select NY-ESO-1 TCR T cells based on their activation kinetics, using the eGFP reporter expressed downstream of the TCR signaling pathway[69]. Interestingly, we noticed that among all of the positive pairs analyzed (NY-ESO-1 TCR/NY-ESO-1$^+$ target cells) only about 2/3 were activated, which also happened in bulk (though to a

Author Manuscript Author Manuscript Author Manuscript Author Manuscript

lesser extent, with a maximum of 75% TCR T cells activated after 9 hours). This could reflect the heterogeneity of the T cell and/or tumor cell population and might be due to the loss of the transgene expression following recombination events in the genome that are well described following lentiviral transduction, either of the TCR, the eGFP reporter or the HLA/antigen complex. The percent of activated cells is slightly more in bulk compared to in droplets probably because the probability for a TCR T cell to meet a target cell expressing the antigen is higher. In addition, similar to bulk data, we observed from our droplet data that NY-ESO-1 TCR T cells were more strongly activated when they were encapsulated with more than one NY-ESO-1$^+$ target cell, particularly at an early time-point (3 hours) (**data not shown**). Having more target cells increased the chances of contact and activation of the TCR, especially if target cells lost the HLA/NY-ESO-1 complex. In addition, crosslinking of multiple TCR molecules on one T cell leads to stronger intracellular signaling, therefore to stronger eGFP expression.

By using a relatively low intensity threshold coupled with kinetics analysis, we increased our sensitivity without diminishing the specificity. Our data showed that we missed three times more true positives when using a more stringent threshold. This illustrates the advantage of kinetics and real time monitoring over end-point analysis in identifying true positive cell clones while limiting false positives.

When comparing droplet-based assays to profile T cell functions, multiplexed reporters can be used to obtain a more comprehensive picture of T cell response. For instance, Steinberger's team has developed T cell reporters where the activity of key transcription factors in T cell activation (NF-κB, NFAT and AP-1) can be simultaneously measured[74]. The use of those reporter cells could be extended to screen for TCR or CAR libraries[75, 76] and to study the response of the CAR/TCR-transgenic reporters to various co-stimulatory/co-inhibitory signals[77]. In addition, future work will also consider droplet-based assay chemistries that can measure, for example, granzyme B production for CD8$^+$ T cell killing activity upon cognate antigen recognition, cytokine release for CD4$^+$ or CD8$^+$ T cells, and use Fura-2 to monitor early activation of primary T cells through elevation of intracellular calcium concentration.

Despite its high spatiotemporal control and ability to analyze and recover single cells, our microfluidic system has several limitations. First, the co-encapsulation efficiency of T cells and tumor cells remains low due to Poisson encapsulation statistics; the probability to get one TCR T cell and one or more target cell(s) in droplet is approximately 20%. Different methods have been developed to increase the co-encapsulation efficiency, including close-packed or inertial ordering before droplet generation[78–81], droplet enrichment by active sorting and downstream merging[82, 83], and droplet co-encapsulation by pico-injection[84], which we will explore in the future. During droplet incubation on the iFDA, observed evaporation was associated with a decrease in droplet size due to PDMS permeability to the vapor of aqueous solutions. To reduce droplet evaporation, humidity was increased within the live cell chamber and PDMS chips were made with greater thickness (>8mm) than first models. Evaporation can be further prevented in the future by using alternative materials such as thermoplastics (PMMA, PC, COC, *etc.*) to fabricate microfluidic chips[85]. In addition, cell movement in droplets and the fact that cells could be on a different focal plane

Author Manuscript Author Manuscript Author Manuscript Author Manuscript

during the real-time monitoring could affect fluorescence intensity measurement. To overcome that issue, we performed z-stack series and did intensity analysis on the image with the optimal focus. However, this method is time-consuming and requires large amount of storage memory. Thus, strategies to position the cells within the same focal plane[59] or applying multi-color bead-based normalization[60] in droplets is critical for quantifying cell functions based on fluorescence measurements and for mitigating issues of photobleaching. The total number of trapping wells and the low frequency of the laser-based sorting (~0.001Hz) limit the throughput of our system. Indeed, it currently takes about fifteen minutes to sort one droplet (two nanoseconds of laser triggering, ten minutes to generate the heat-induced cavitation that expels the droplet out of the well, and < 5 minutes to recover the droplet into a PCR tube). However, this system allows for robust tracking of individual droplets while preserving the cell viability and RNA integrity, as the UV laser is only triggered for a few nanoseconds and 100 μm apart from the cell itself. Future work will integrate new components such as dielectrophoresis (DEP) based sorting in order to improve the throughput to identify rare clones from libraries of million(s) of T cells per run[86, 87]. Finally, an automatic single droplet dispensing system needs to be developed to increase the efficiency of single cell recovery for downstream analysis.

Conclusions

Our technology of functional and dynamic screening of single T cells allows to identify rare clones masked by a large heterogeneity of broad immune cell repertoire and can facilitate and accelerate future TCR discovery and development of T cell therapies. With this technique, primary T cells isolated from a primary tumor or engineered using a TCR or CAR library can be analyzed to identify the rare clones of interest that support a strong and sustained anti-tumor response, potentially in a personalized fashion. Moreover, the ability to dissect complex heterogeneity of immune cells and their interactions with other cell types can help elucidate the underlying mechanisms of immunity in homeostasis, disease and treatment. For example, T cell response to immune checkpoint inhibitors could be visualized at the single cell level, which enables to precisely analyze their mechanisms of action and understand how tumor heterogeneity contribute to resistance to treatments. Finally, this platform technology can be extended to functional analysis of B-cell receptor (BCR) repertoire[88, 89], stem cells, circulating tumor cells or other rare cell types.

Supplementary Material

Refer to Web version on PubMed Central for supplementary material.

Acknowledgements

The authors would like to thank Chih Chun Yu for his help in finishing the TCR T cell activation experiments in droplets and assistance in droplet sorting, and Stephanie Wong for her help in single cell PCR work. The authors are also grateful to Cassandra Kiyomi Davis for her support in culturing the cells and performing cell viability test from droplets. This work is supported by the NIH (1DP2CA195763 and R21CA219225), and Amberstone Biosciences LLC: No. AB-208317.

Author Manuscript Author Manuscript Author Manuscript Author Manuscript

Bibliographic references & notes

1. Lim WA and June CH, Cell, 2017, 168, 724–740. [PubMed: 28187291]
2. Gee MH, Han A, Lofgren SM, Beausang JF, Mendoza JL, Birnbaum ME, Bethune MT, Fischer S, Yang XB, Gomez-Eerland R, Bingham DB, Sibener LV, Fernandes RA, Velasco A, Baltimore D, Schumacher TN, Khatri P, Quake SR, Davis MM and Garcia KC, Cell, 2018, 172, 549-+. [PubMed: 29275860]
3. Zhou PH, Shaffer DR, Arias DAA, Nakazaki Y, Pos W, Torres AJ, Cremasco V, Dougan SK, Cowley GS, Elpek K, Brogdon J, Lamb J, Turley SJ, Ploegh HL, Root DE, Love JC, Dranoff G, Hacohen N, Cantor H and Wucherpfennig KW, Nature, 2014, 506, 52-+. [PubMed: 24476824]
4. June CH and Sadelain M, New Engl J Med, 2018, 379, 64–73. [PubMed: 29972754]
5. Johnson LA, Heemskerk B, Powell DJ, Cohen CJ, Morgan RA, Dudley ME, Robbins PF and Rosenberg SA, J Immunol, 2006, 177, 6548–6559. [PubMed: 17056587]
6. Li Y, Moysey R, Molloy PE, Vuidepot AL, Mahon T, Baston E, Dunn S, Liddy N, Jacob J, Jakobsen BK and Boulter JM, Nat Biotechnol, 2005, 23, 349–354. [PubMed: 15723046]
7. Castellarin M, Watanabe K, June CH, Kloss CC and Posey AD, Gene Ther, 2018, 25, 165–175. [PubMed: 29880908]
8. Garber K, Nat Biotechnol, 2018, 36, 215–219. [PubMed: 29509745]
9. Laydon DJ, Bangham CRM and Asquith B, Philos T R Soc B, 2015, 370.
10. Kitaura K, Shini T, Matsutani T and Suzuki R, Bmc Immunol, 2016, 17.
11. Mamedov IZ, Britanova OV, Bolotin DA, Chkalina AV, Staroverov DB, Zuyagin IV, Kotlobay AA, Turchaninova MA, Fedorenko DA, Novik AA, Sharonov GV, Lukyanov S, Chudakov DM and Lebedev YB, Embo Mol Med, 2011, 3, 201–207. [PubMed: 21374820]
12. Lu Y, Xue Q, Eisele MR, Sulistijo ES, Brower K, Han L, Amir ED, Pe'er D, Miller-Jensen K and Fan R, P Natl Acad Sci USA, 2015, 112, E607–E615.
13. Malissen B, Gregoire C, Malissen M and Roncagalli R, Nat Immunol, 2014, 15, 790–797. [PubMed: 25137453]
14. Ma C, Fan R, Ahmad H, Shi QH, Comin-Anduix B, Chodon T, Koya RC, Liu CC, Kwong GA, Radu CG, Ribas A and Heath JR, Nat Med, 2011, 17, 738–U133. [PubMed: 21602800]
15. Mahata B, Zhang XW, Kolodziejczyk AA, Proserpio V, Haim-Vilmovsky L, Taylor AE, Hebenstreit D, Dingler FA, Moignard V, Gottgens B, Arlt W, McKenzie ANJ and Teichmann SA, Cell Rep, 2014, 7, 1130–1142. [PubMed: 24813893]
16. Peine M, Rausch S, Helmstetter C, Frohlich A, Hegazy AN, Kuhl AA, Grevelding CG, Hofer T, Hartmann S and Lohning M, Plos Biol, 2013, 11.
17. Linnemann C, Heemskerk B, Kvistborg P, Kluin RJC, Bolotin DA, Chen XJ, Bresser K, Nieuwland M, Schotte R, Michels S, Gomez-Eerland R, Jahn L, Hombrink P, Legrand N, Shu CJ, Mamedov IZ, Velds A, Blank CU, Haanen JBAG, Turchaninova MA, Kerkhoven RM, Spits H, Hadrup SR, Heemskerk MHM, Blankenstein T, Chudakov DM, Bendle GM and Schumacher TNM, Nat Med, 2013, 19, 1534-+. [PubMed: 24121928]
18. Gejman RS, Dao T and Scheinberg DA, Blood, 2017, 130.
19. Eisenstein M, Nature, 2006, 441, 1179-+. [PubMed: 16810261]
20. De Simone M, Rossetti G and Pagani M, Front Immunol, 2018, 9.
21. Stubbington MJT, Rozenblatt-Rosen O, Regev A and Teichmann SA, Science, 2017, 358, 58–63. [PubMed: 28983043]
22. Staudt N, Muller-Sienerth N and Wright GJ, Biochem Bioph Res Co, 2014, 445, 785–790.
23. Shembekar N, Chaipan C, Utharala R and Merten CA, Lab Chip, 2016, 16, 1314–1331. [PubMed: 27025767]
24. Mazutis L, Gilbert J, Ung WL, Weitz DA, Griffiths AD and Heyman JA, Nat Protoc, 2013, 8, 870–891. [PubMed: 23558786]
25. Adler AS, Mizrahi RA, Spindler MJ, Adams MS, Asensio MA, Edgar RC, Leong J, Leong R, Roalfe L, White R, Goldblatt D and Johnson DS, Mabs-Austin, 2017, 9, 1282–1296.
26. Hatch AC, Fisher JS, Tovar AR, Hsieh AT, Lin R, Pentoney SL, Yang DL and Lee AP, Lab Chip, 2011, 11, 3838–3845. [PubMed: 21959960]

Author Manuscript Author Manuscript Author Manuscript Author Manuscript

27. Williams R, Peisajovich SG, Miller OJ, Magdassi S, Tawfik DS and Griffiths AD, Nat Methods, 2006, 3, 545–550. [PubMed: 16791213]
28. Klein AM, Mazutis L, Akartuna I, Tallapragada N, Veres A, Li V, Peshkin L, Weitz DA and Kirschner MW, Cell, 2015, 161, 1187–1201. [PubMed: 26000487]
29. DeKosky BJ, Ippolito GC, Deschner RP, Lavinder JJ, Wine Y, Rawlings BM, Varadarajan N, Giesecke C, Dorner T, Andrews SF, Wilson PC, Hunicke-Smith SP, Willson CG, Ellington AD and Georgiou G, Nat Biotechnol, 2013, 31, 166–169. [PubMed: 23334449]
30. Tang FC, Barbacioru C, Wang YZ, Nordman E, Lee C, Xu NL, Wang XH, Bodeau J, Tuch BB, Siddiqui A, Lao KQ and Surani MA, Nat Methods, 2009, 6, 377–U386. [PubMed: 19349980]
31. Turchaninova MA, Britanova OV, Bolotin DA, Shugay M, Putintseva EV, Staroverov DB, Sharonov G, Shcherbo D, Zvyagin IV, Mamedov IZ, Linnemann C, Schumacher TN and Chudakov DM, Eur J Immunol, 2013, 43, 2507–2515. [PubMed: 23696157]
32. Lim SW and Abate AR, Lab Chip, 2013, 13, 4563–4572. [PubMed: 24146020]
33. Macosko EZ, Basu A, Satija R, Nemesh J, Shekhar K, Goldman M, Tirosh I, Bialas AR, Kamitaki N, Martersteck EM, Trombetta JJ, Weitz DA, Sanes JR, Shalek AK, Regev A and McCarroll SA, Cell, 2015, 161, 1202–1214. [PubMed: 26000488]
34. Konry T, Dominguez-Villar M, Baecher-Allan C, Hafler DA and Yarmush ML, Biosens Bioelectron, 2011, 26, 2707–2710. [PubMed: 20888750]
35. Diercks AH, Ozinsky A, Hansen CL, Spotts JM, Rodriguez DJ and Aderem A, Anal Biochem, 2009, 386, 30–35. [PubMed: 19133224]
36. Han Q, Bagheri N, Bradshaw EM, Hafler DA, Lauffenburger DA and Love JC, P Natl Acad Sci USA, 2012, 109, 1607–1612.
37. Chokkalingam V, Tel J, Wimmers F, Liu X, Semenov S, Thiele J, Figdor CG and Huck WTS, Lab Chip, 2013, 13, 4740–4744. [PubMed: 24185478]
38. Sarkar S, Sabhachandani P, Ravi D, Potdar S, Purvey S, Beheshti A, Evens AM and Konry T, Front Immunol, 2017, 8.
39. Sarkar S, Sabhachandani P, Stroopinsky D, Palmer K, Cohen N, Rosenblatt J, Avigan D and Konry T, Biomicrofluidics, 2016, 10.
40. Konry T, Golberg A and Yarmush M, Sci Rep-Uk, 2013, 3.
41. Jin SH, Lee SS, Lee B, Jeong SG, Peter M and Lee CS, Anal Chem, 2017, 89, 9722–9729. [PubMed: 28823147]
42. Yamanaka YJ, Berger CT, Sips M, Cheney PC, Alter G and Love JC, Integr Biol-Uk, 2012, 4, 1175–1184.
43. Junkin M, Kaestli AJ, Cheng Z, Jordi C, Albayrak C, Hoffmann A and Tay S, Cell Rep, 2016, 15, 411–422. [PubMed: 27050527]
44. Chen B, Lim SW, Kannan A, Alford SC, Sunden F, Herschlag D, Dimov IK, Baer TM and Cochran JR, Nat Chem Biol, 2016, 12, 76-+. [PubMed: 26641932]
45. Fallah-Araghi A, Baret JC, Ryckelynck M and Griffiths AD, Lab Chip, 2012, 12, 882–891. [PubMed: 22277990]
46. Brouzes E, Medkova M, Savenelli N, Marran D, Twardowski M, Hutchison JB, Rothberg JM, Link DR, Perrimon N and Samuels ML, P Natl Acad Sci USA, 2009, 106, 14195–14200.
47. Varadarajan N, Kwon DS, Law KM, Ogunniyi AO, Anahtar MN, Richter JM, Walker BD and Love JC, P Natl Acad Sci USA, 2012, 109, 3885–3890.
48. Sarkar S, Motwani V, Sabhachandani P, Cohen N and Konry T, J Clin Cell Immunol, 2015, 6.
49. Pavesi A, Tan AT, Koh S, Chia A, Colombo M, Antonecchia E, Miccolis C, Ceccarello E, Adriani G, Raimondi MT, Kamm RD and Bertoletti A, Jci Insight, 2017, 2.
50. Xue Q, Bettini E, Paczkowski P, Ng C, Kaiser A, McConnell T, Kodrasi O, Quigley MF, Heath J, Fan R, Mackay S, Dudley ME, Kassim SH and Zhou J, J Immunother Cancer, 2017, 5.
51. Fitzgerald V, Manning B, O'Donnell B, O'Reilly B, O'Sullivan D, O'Kennedy R and Leonard P, Anal Chem, 2015, 87, 997–1003. [PubMed: 25479183]
52. El Debs B, Utharala R, Balyasnikova IV, Griffiths AD and Merten CA, P Natl Acad Sci USA, 2012, 109, 11570–11575.

Author Manuscript Author Manuscript Author Manuscript Author Manuscript

53. Sista RS, Eckhardt AE, Srinivasan V, Pollack MG, Palanki S and Pamula VK, Lab Chip, 2008, 8, 2188–2196. [PubMed: 19023486]
54. Love JC, Ronan JL, Grotenbreg GM, van der Veen AG and Ploegh HL, Nat Biotechnol, 2006, 24, 703–707. [PubMed: 16699501]
55. Skelley AM, Kirak O, Suh H, Jaenisch R and Voldman J, Nat Methods, 2009, 6, 147–152. [PubMed: 19122668]
56. Singhal A, Haynes CA and Hansen CL, Anal Chem, 2010, 82, 8671–8679. [PubMed: 20857931]
57. Adler AS, Bedinger D, Adams MS, Asensio MA, Edgar RC, Leong R, Leong J, Mizrahi RA, Spindler MJ, Bandi SR, Huang HC, Tawde P, Brams P and Johnson DS, Mabs-Austin, 2018, 10, 431–443.
58. Adler AS, Mizrahi RA, Spindler MJ, Adams MS, Asensio MA, Edgar RC, Leong J, Leong R and Johnson DS, Mabs-Austin, 2017, 9, 1270–1281.
59. Eyer K, Doineau RCL, Castrillon CE, Briseno-Roa L, Menrath V, Mottet G, England P, Godina A, Brient-Litzler E, Nizak C, Jensen A, Griffiths AD, Bibette J, Bruhns P and Baudry J, Nat Biotechnol, 2017, 35, 977-+. [PubMed: 28892076]
60. Shembekar N, Hu HX, Eustace D and Merten CA, Cell Rep, 2018, 22, 2206–2215. [PubMed: 29466744]
61. Clausell-Tormos J, Lieber D, Baret JC, El-Harrak A, Miller OJ, Frenz L, Blouwolff J, Humphry KJ, Koster S, Duan H, Holtze C, Weitz DA, Griffiths AD and Merten CA, Chem Biol, 2008, 15, 875–875.
62. Perez-Garnarra S, Hattara L, Batra G, Saviranta P and Lamminmaki U, Methods, 2017, 116, 43–50. [PubMed: 27956240]
63. McDaniel JR, DeKosky BJ, Tanno H, Ellington AD and Georgiou G, Nat Protoc, 2016, 11, 429–442. [PubMed: 26844430]
64. Rapoport AP, Stadtmauer EA, Binder-Scholl GK, Goloubeva O, Vogl DT, Lacey SF, Badros AZ, Garfall A, Weiss B, Finklestein J, Kulikovskaya I, Sinha SK, Kronsberg S, Gupta M, Bond S, Melchiori L, Brewer JE, Bennett AD, Gerry AB, Pumphrey NJ, Williams D, Tayton-Martin HK, Ribeiro L, Holdich T, Yanovich S, Hardy N, Yared J, Kerr N, Philip S, Westphal S, Siegel DL, Levine BL, Jakobsen BK, Kalos M and June CH, Nat Med, 2015, 21, 914–921. [PubMed: 26193344]
65. Gnjatic S, Nishikawa H, Jungbluth AA, Gure AO, Ritter G, Jager E, Chen YT and Old LJ, Adv Cancer Res, 2006, 95, 1–30. [PubMed: 16860654]
66. Hunder NN, Wallen H, Cao J, Hendricks DW, Reilly JZ, Rodmyre R, Jungbluth A, Gnjatic S, Thompson JA and Yee C, N Engl J Med, 2008, 358, 2698–2703. [PubMed: 18565862]
67. Duffy DC, McDonald JC, Schueller OJA and Whitesides GM, Anal Chem, 1998, 70, 4974–4984. [PubMed: 21644679]
68. Labanieh L, Nguyen TN, Zhao WA and Kang DK, Micromachines-Basel, 2015, 6, 1469–1482. [PubMed: 27134760]
69. Hooijberg E, Bakker AQ, Ruizendaal JJ and Spits H, Blood, 2000, 96, 459–466. [PubMed: 10887106]
70. Cohen CJ, Li YF, El-Gamil M, Robbins PF, Rosenberg SA and Morgan RA, Cancer Res, 2007, 67, 3898–3903. [PubMed: 17440104]
71. Park SY, Wu TH, Chen Y, Teitell MA and Chiou PY, Lab Chip, 2011, 11, 1010–1012. [PubMed: 21290045]
72. Stahlberg A and Kubista M, Expert Rev Mol Diagn, 2014, 14, 323–331. [PubMed: 24649819]
73. Dura B, Dougan SK, Barisa M, Hoehl MM, Lo CT, Ploegh HL and Voldman J, Nat Commun, 2015, 6.
74. Rosskopf S, Jutz S, Neunkirchner A, Candia MR, Jahn-Schmid B, Bohle B, Pickl WF and Steinberger P, Sci Rep-Uk, 2016, 6.
75. Birkholz K, Hofmann C, Hoyer S, Schulz B, Harrer T, Kampgen E, Schuler G, Dorrie J and Schaft N, J Immunol Methods, 2009, 346, 45–54. [PubMed: 19427315]
76. Aarnoudse CA, Kruse M, Konopitzky R, Brouwenstijn N and Schrier PI, Int J Cancer, 2002, 99, 7–13. [PubMed: 11948485]

Author Manuscript Author Manuscript Author Manuscript Author Manuscript

77. Rosskopf S, Leitner J, Paster W, Morton LT, Hagedoorn RS, Steinberger P and Heemskerk MHM, Oncotarget, 2018, 9, 17608–17619. [PubMed: 29707134]
78. Abate AR, Chen CH, Agresti JJ and Weitz DA, Lab Chip, 2009, 9, 2628–2631. [PubMed: 19704976]
79. Edd JF, Di Carlo D, Humphry KJ, Koster S, Irimia D, Weitz DA and Toner M, Lab Chip, 2008, 8, 1262–1264. [PubMed: 18651066]
80. Lagus TP and Edd JF, Rsc Adv, 2013, 3, 20512–20522.
81. Schoeman RM, Kemna EWM, Wolbers F and van den Berg A, Electrophoresis, 2014, 35, 385–392. [PubMed: 23856757]
82. Chung MT, Nunez D, Cai DW and Kurabayashi K, Lab Chip, 2017, 17, 3664–3671. [PubMed: 28967663]
83. Hu HX, Eustace D and Merten CA, Lab Chip, 2015, 15, 3989–3993. [PubMed: 26313441]
84. Schoendube J, Wright D, Zengerle R and Koltay P, Biomicrofluidics, 2015, 9.
85. Ren KN, Zhou JH and Wu HK, Accounts Chem Res, 2013, 46, 2396–2406.
86. Xi HD, Zheng H, Guo W, Ganan-Calvo AM, Ai Y, Tsao CW, Zhou J, Li WH, Huang YY, Nguyen NT and Tan SH, Lab Chip, 2017, 17, 751–771. [PubMed: 28197601]
87. Frenzel D and Merten CA, Lab Chip, 2017, 17, 1024–1030. [PubMed: 28232987]
88. Seah YFS, Hu HX and Merten CA, Mol Aspects Med, 2018, 59, 47–61. [PubMed: 28927942]
89. Fitzgerald V and Leonard P, Methods, 2017, 116, 34–42. [PubMed: 27864085]

Author Manuscript Author Manuscript Author Manuscript Author Manuscript

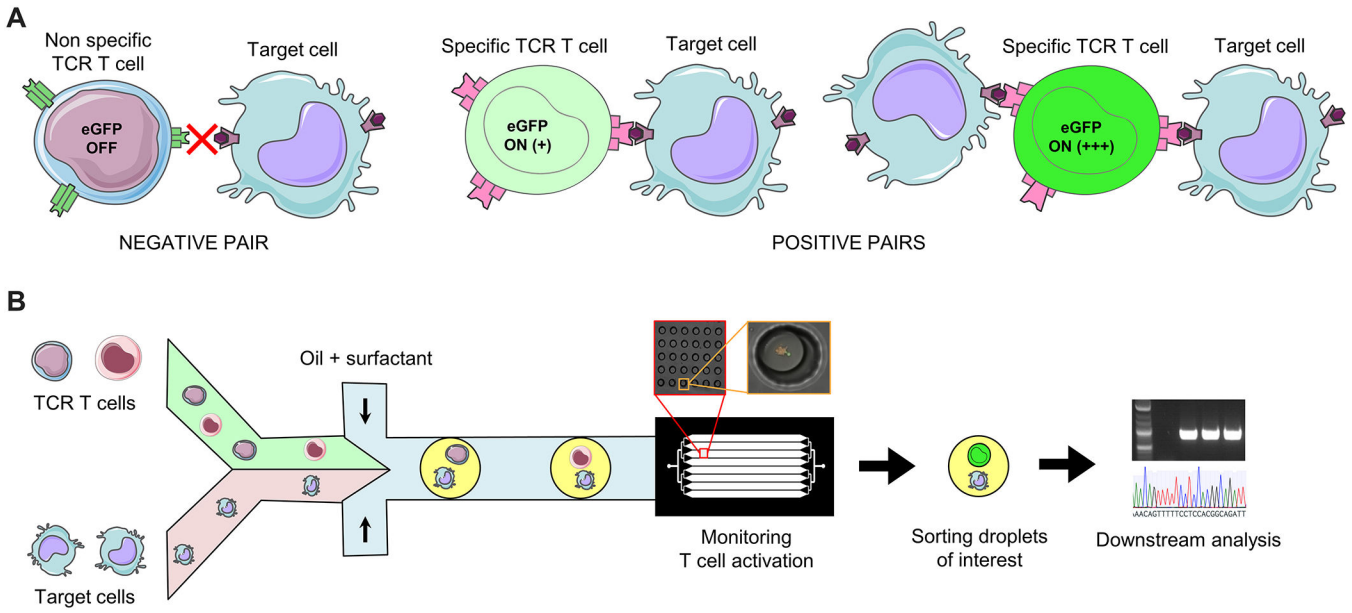

Figure 1: A droplet based platform allows for the screening of specific TCR T cells that recognize target tumor antigens.

A) Non-specific TCR T cells (MART-1 TCR T cells) do not recognize the target cells expressing the NY-ESO-1 antigen (negative pair, left panel) whereas specific TCR T cells (NY-ESO-1 TCR T cells) get activated upon recognition of their cognate antigen, triggering the expression of eGFP (positive pairs, right panel). TCR T cells that interact with multiple target cells exhibit stronger activation. B) Schematic of our single cell screening workflow. Specific and non specific TCR T cells were mixed and encapsulated in droplets together with target cells before being loaded on a device to monitor T cell activation. After analysis, droplets containing activated T cells were sorted for downstream molecular analysis (PCR and sequencing of the TCR sequence).

Author Manuscript Author Manuscript Author Manuscript Author Manuscript

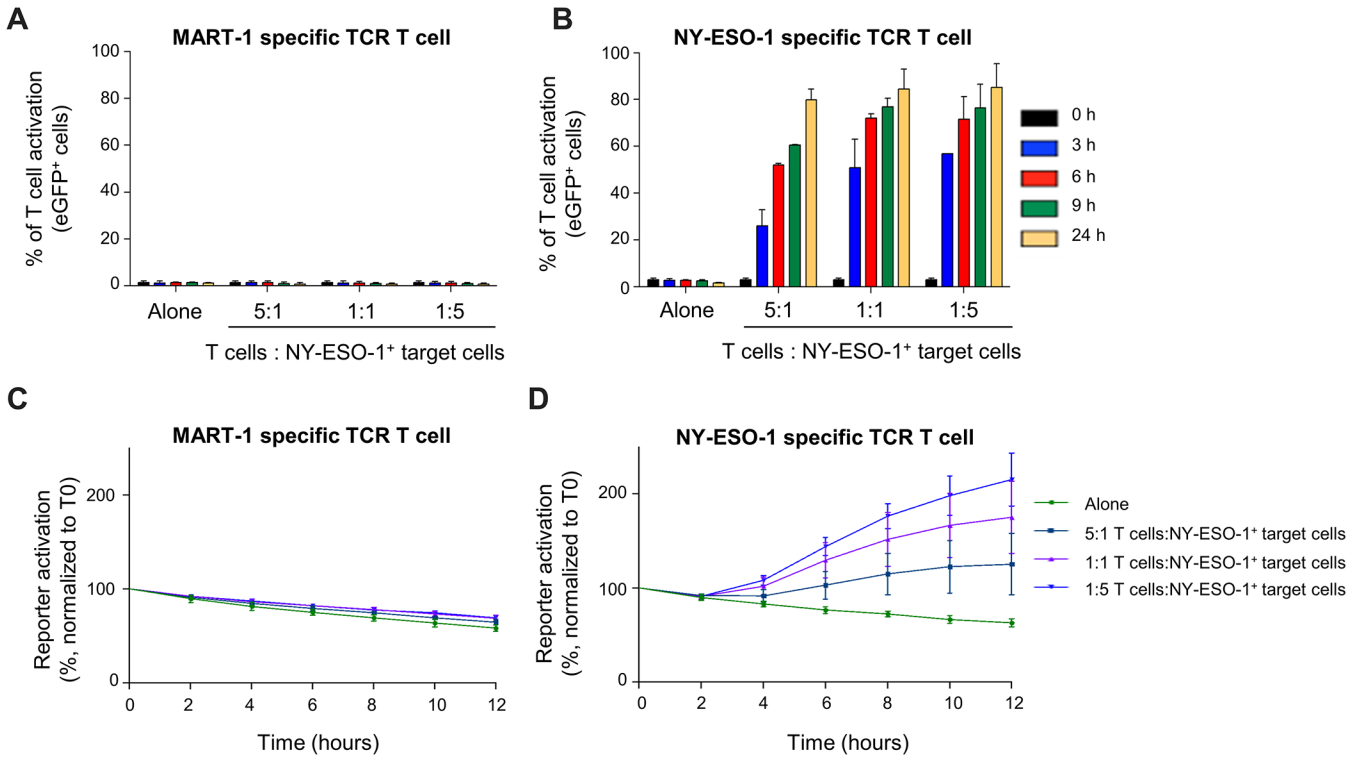

Figure 2: NY-ESO-1 TCR T cells specifically activate in the presence of NY-ESO-1$^+$ target cells in a time and target cell concentration dependent fashion in bulk.

A) MART-1 specific TCR cells and B) NY-ESO-1 TCR cells were plated at different TCR T cell: target cell ratios (5:1, 1:1 and 1:5) with a fixed number of TCR T cells. The percentage of cells that became activated was measured using flow cytometry by counting eGFP$^+$ cells at 0, 3, 6, 9 and 24 hours. The activation kinetics was analyzed over 12 hours by measuring the total fluorescence emitted from the eGFP every 2 hours on a plate reader for both C) the negative pair and D) the positive pair.

Author Manuscript Author Manuscript Author Manuscript Author Manuscript

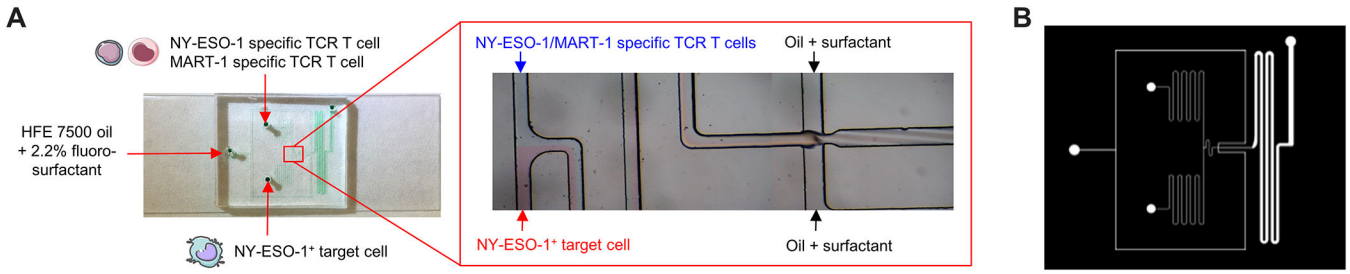

Figure 3: The droplet microfluidic device used to generate 120 μm-diameter droplets containing co-encapsulated TCR T cells and target cells.

A) A flow-focusing droplet generator was used to generate aqueous in oil droplets. The two symmetric inlets were loaded with cell solutions containing food dyes for better clarity: blue for TCR cells and red for target cells, before being mixed at the junction where the aqueous phase got pinched by HFE 7500 oil containing 2.2% by weight fluoro-surfactant (PFPE 5000-PEG900) to generate droplets. B) Mask design of flow-focusing droplet generator.

Author Manuscript Author Manuscript Author Manuscript Author Manuscript

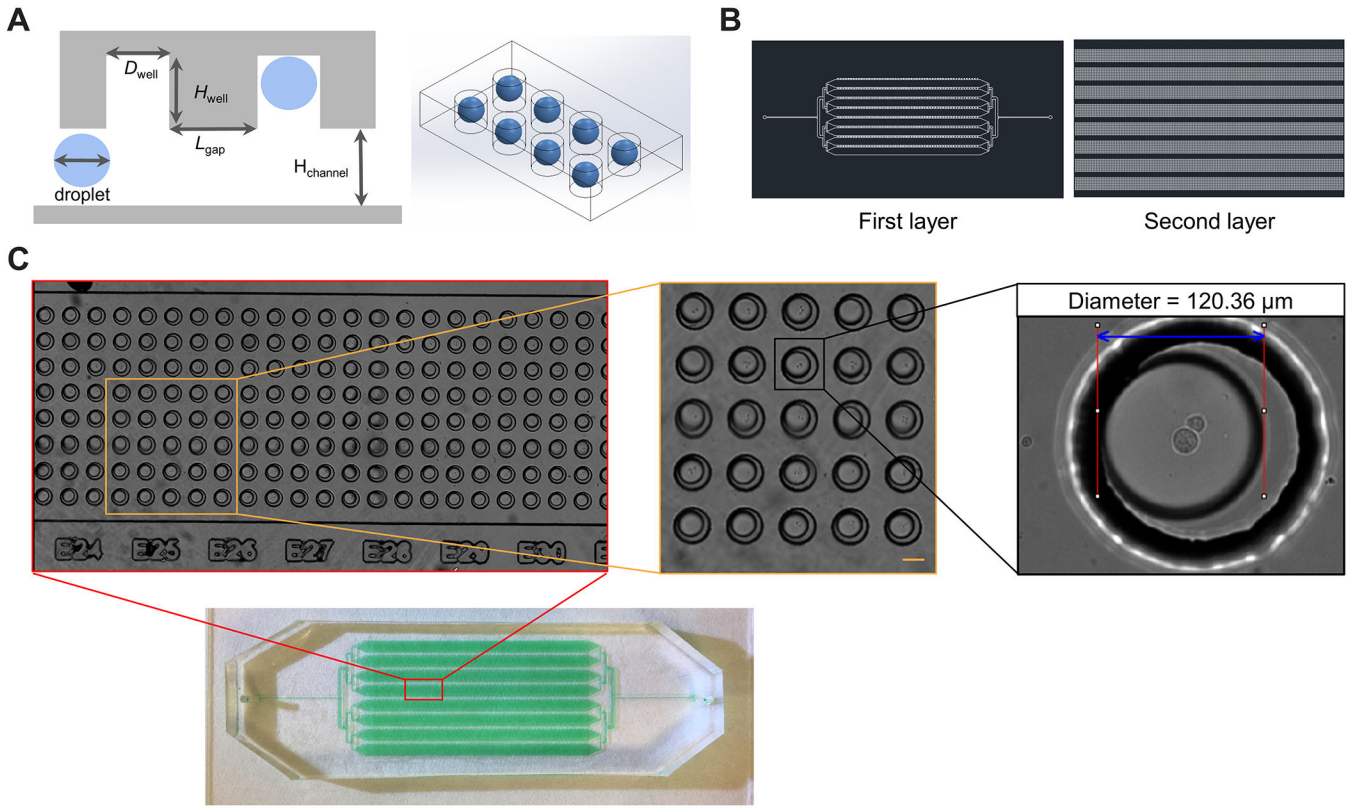

Figure 4: Generated droplets are loaded into a floating droplet array (iFDA) containing 10,368 trapping wells for imaging.

A) Each well has a diameter of D_{well}=140µm, and a height of H_{well}=130µm to ensure of single droplet trapping. The gap length between two adjacent wells is L_{gap}=100µm to maximize the number of wells. The channel height $H_{channel}$=150µm is set slightly larger than the droplet diameter to allow single layer of droplets to pass through the chamber. B) Mask design of the iFDA chip with a two-layer fabrication. The entire chip was divided into eight sections of 1,296 wells to reduce dead zones. C) Droplets occupied all the trapping wells after the loading and flushing of the extra droplets. Right image: higher magnification of a trapping well containing a 120 µm-diameter droplet with a NY-ESO-1 specific TCR T cell interacting with a target cell. Scale bar: 100µm.

Author Manuscript
Author Manuscript
Author Manuscript
Author Manuscript

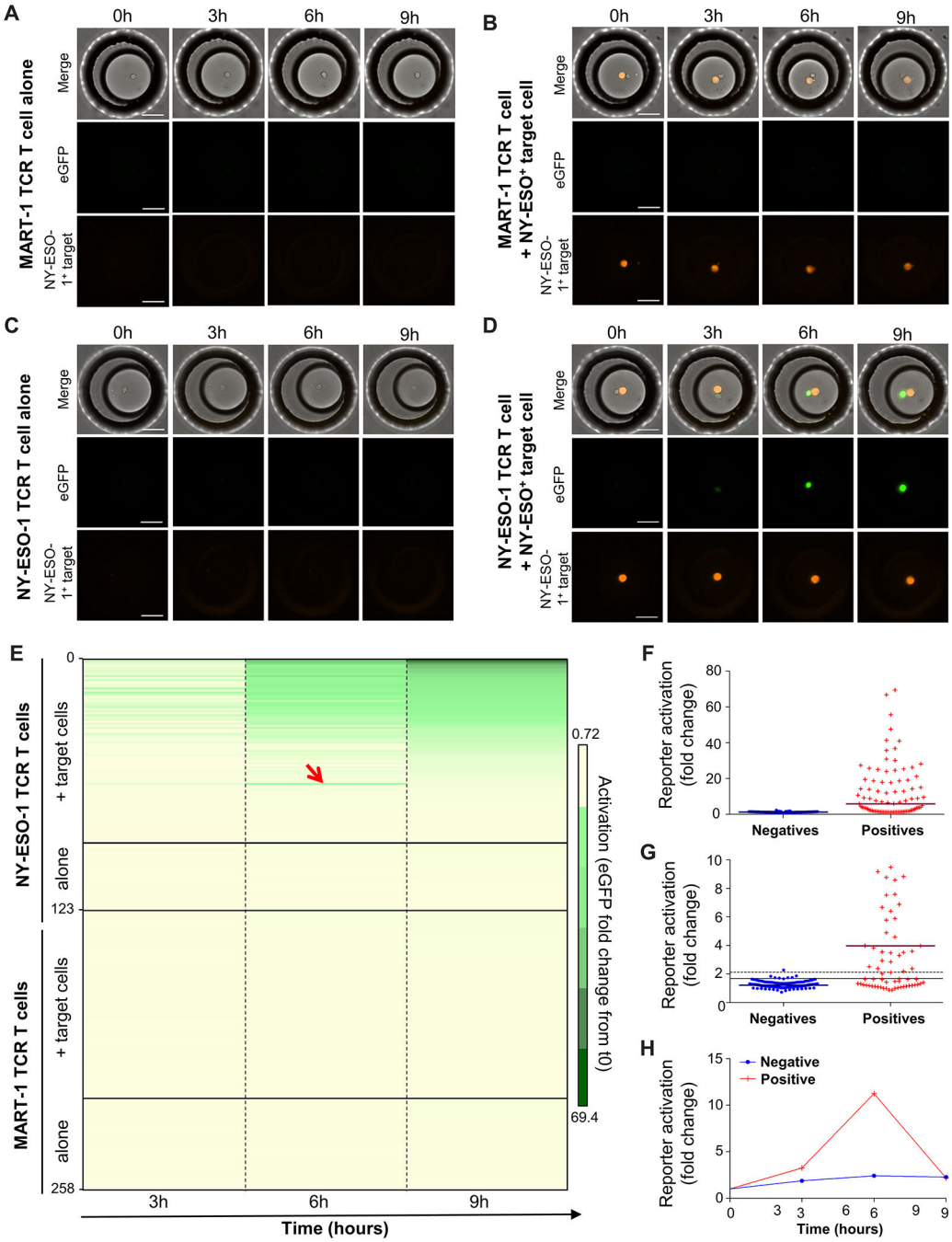

Figure 5: Kinetics of T cell reporter activation is measured in droplets by eGFP expression over time.

Representative microscope images of droplets containing A) MART-1 TCR cells alone, B) MART-1 TCR cells encapsulated in presence of target cells, C) NY-ESO-1 TCR cells alone or D) NY-ESO-1 TCR cells encapsulated in presence of target cells that were imaged over time in the iFDA chip 3, 6 and 9h after encapsulation. Orange: target cells, green: eGFP expressed by activated TCR T cells. Scale bar: 100μm. E) TCR T cell activation was measured by fold increase of eGFP expression compared to T0 for each individual cell. The activation profile of each TCR T cell was plotted in a heat map. Each row represents one

Author Manuscript Author Manuscript Author Manuscript Author Manuscript

TCR T cell, and each column a different time-point. For each group, TCR cells were organized starting from the strongest activation down to the lowest activation (dark green to pale yellow). 90 droplets were analyzed for both the negative and positive pairs, and only half droplets were analyzed for NY-ESO-1 TCR T cells alone and MART-1 TCR T cells alone. The red arrow points out a TCR T cell that was strongly activated after 6 hours, but with signal decreased at 9 hours probably due to a loss of cell viability. (F) Fold increases of eGFP expression at 9 hours (end-point). Each dot or cross represents one TCR T cell and the short line indicates the median of TCR activation. Negatives: MART-1 TCR T cell + target cell(s), positives: NY-ESO-1 TCR T cell + target cell(s). G) Zoom-in of plot F) which shows fold increase of eGFP expression at 9 hours in the low range (up to 10-fold increase). A black dash line shows a stringent threshold (mean of negatives + 4 standard deviations=2.11 fold increase) while a full black line shows a less stringent threshold (mean of negatives + 2 standard deviations=1.89 fold increase). H) Example of activation kinetics for TCR T cells from a negative and a positive pair that have the same end-point activation values, but different activation kinetics.

Author Manuscript
Author Manuscript
Author Manuscript
Author Manuscript

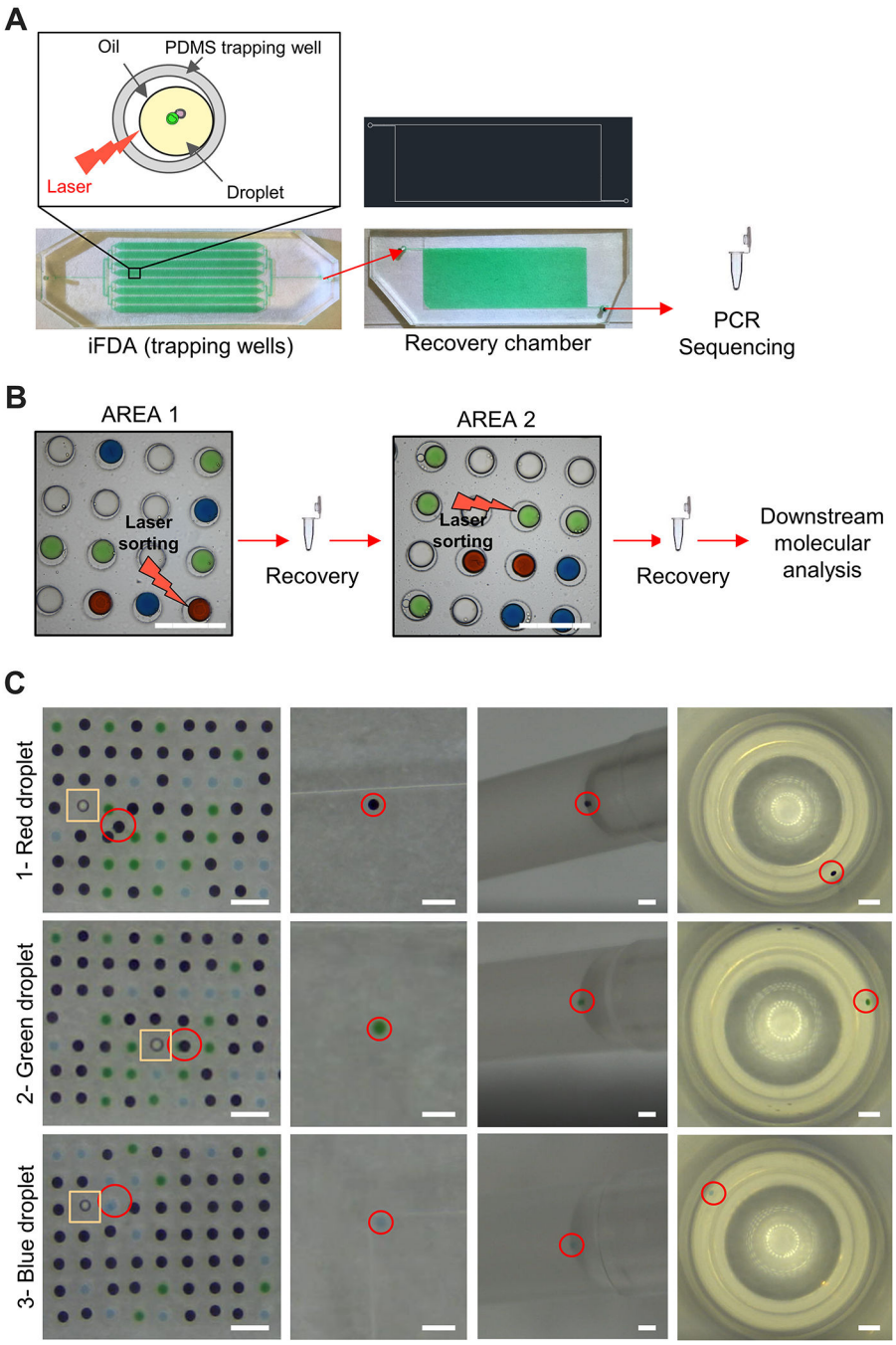

Figure 6: Droplets containing single activated TCR T cell are sorted using laser-based cavitation for downstream molecular analysis.

A) Workflow of single droplet sorting and dispensing. B) To validate droplet tracking, droplets stained with different food dyes (green, blue, red) and droplets without any dye were loaded into iFDA chip and sorted in order of color. Scale bar = 400 μm. C) Example of three droplets that were sequentially sorted and collected in the following order: red, green and blue. Pictures were taken at each step of the process (from left to right): post laser kicking in the iFDA, recovery chamber, pipette tip and PCR tube. The yellow rectangle

indicates the initial well that contained the droplet, and the red circle indicates the kicked droplet floating in the iFDA. Scale bar = 400μm.

Author Manuscript Author Manuscript Author Manuscript Author Manuscript

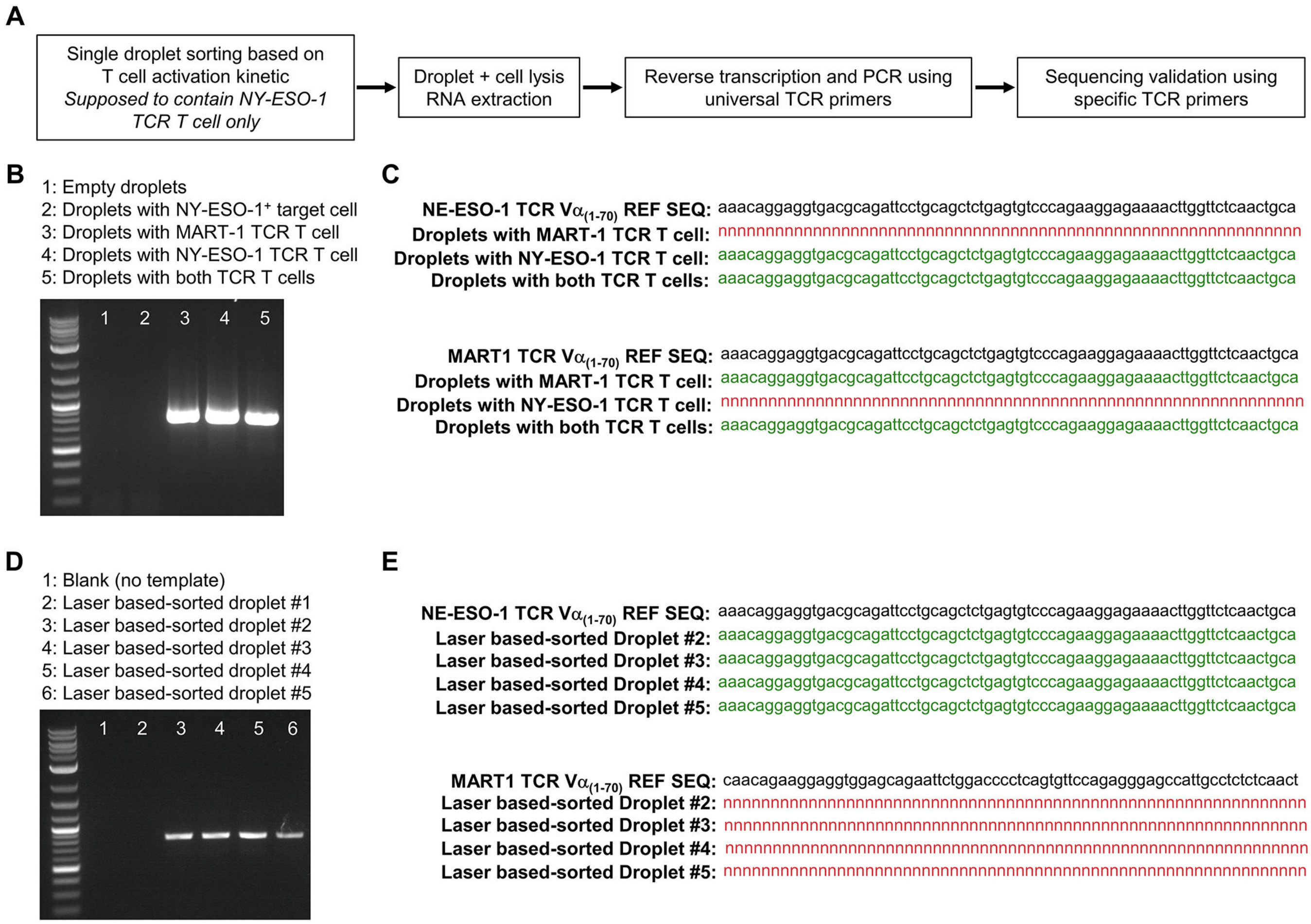

Figure 7: Single cell RT-PCR and sequencing analyses.

A) Workflow of downstream T cell analyses following sorting. B) Gel electrophoresis of various reverse-transcription/PCR products. About 15 droplets were used for each condition. C) Subsequent sequencing data of amplified DNA from lanes 3,4 and 5 in B). D) As a proof of concept, five droplets randomly sorted based on T cell activation kinetics were collected and lysed to extract RNA, then subjected to reverse-transcription and PCR which was analyzed using gel electrophoresis. E) The sequencing data obtained from the purified gel bands in D) confirmed that the sorted droplets only contained NY-ESO-1 TCR and no MART-1 TCR T cells.

Author Manuscript Author Manuscript Author Manuscript Author Manuscript